

Optimizing the efficiency of a periodically poled LNOI waveguide using *in situ* monitoring of the ferroelectric domains

Cite as: Appl. Phys. Lett. **116**, 101104 (2020); doi: 10.1063/1.5142750

Submitted: 17 December 2019 · Accepted: 28 February 2020 ·

Published Online: 10 March 2020




View Online



Export Citation



CrossMark

Yunfei Niu,¹ Chen Lin,¹  Xiaoyue Liu,² Yan Chen,¹ Xiaopeng Hu,^{1,a)}  Yong Zhang,¹  Xinlun Cai,^{2,a)} Yan-Xiao Gong,¹ Zhenda Xie,^{1,a)} and Shining Zhu¹

AFFILIATIONS

¹National Laboratory of Solid State Microstructures, College of Engineering and Applied Sciences, College of Electronic Science and Engineering, and School of Physics, Nanjing University, Nanjing 210093, China

²State Key Laboratory of Optoelectronic Materials and Technologies and School of Electronics and Information Technology, Sun Yat-sen University, Guangzhou 510275, China

^{a)}Authors to whom correspondence should be addressed: xphu@nju.edu.cn, caixlun5@mail.sysu.edu.cn, and xiezhenda@nju.edu.cn

ABSTRACT

Lithium niobate on insulator (LNOI) is a unique platform for integrated photonic applications and especially for high-efficiency nonlinear frequency converters because of the strong optical field confinement. In this work, we fabricated a 6-mm-long periodically poled LNOI ridge waveguide with an optimized duty cycle (50:50) using an active domain structure monitoring method. The performance of the single-pass second-harmonic generation and difference-frequency generation in the nanophotonic waveguide was characterized, and the normalized conversion efficiencies were $\sim 80\%$ of the theoretical values. These high-quality frequency conversion devices can pave the way for the application of LNOI in nonlinear integrated photonics.

Published under license by AIP Publishing. <https://doi.org/10.1063/1.5142750>

The lithium niobate on insulator (LNOI) platform has drawn increasing attention in recent years. LNOI inherits the excellent material properties of lithium niobate (LiNbO_3) single crystals, such as a wide low-loss transparency window, a strong electro-optic (EO) coefficient,¹ and high second-order nonlinearity.² Moreover, an LNOI platform offers stronger optical confinement compared to conventional weakly confining LiNbO_3 waveguides, such as proton exchanged and titanium in-diffused waveguides,^{3,4} which leads to improved optical signal processing capabilities and enhanced light-matter interactions. Because of these advantages, photonic devices based on LNOI can be more compact and efficient. LNOI has been employed to construct many photonic devices, including high-performance LiNbO_3 integrated EO modulators working at CMOS-compatible voltages,^{5,6} ultrahigh-efficiency frequency converters,^{7,8} high-Q micro-resonators,⁹ and photonic crystal micro-cavities.¹⁰

LiNbO_3 has been widely used for second-order nonlinear frequency conversion in nonlinear optics because of its high second-order nonlinear coefficient. To realize efficient frequency conversion in LNOI waveguides, phase-matching is a key aspect. To date, several

schemes have been used to achieve phase-matching in LNOI-based nonlinear optical elements, such as modal phase matching,^{11–13} metasurface-assisted phase-matching,¹⁴ and quasi-phase matching (QPM). Among these methods, quasi-phase-matched LNOI waveguides can offer several advantages such as phase-matching arbitrary second-order nonlinear optical processes within the transparency range of the crystal, access to the largest nonlinear coefficient, and phase-matching of interactions between the TE_{00} modes that exhibit the tightest mode confinement. Periodically poled ferroelectric domain structures have been fabricated on LNOI platforms, and they have been implemented to demonstrate quasi-phase-matched second-order nonlinear processes such as second-harmonic generation (SHG),^{7,15–17} sum-frequency generation (SFG),¹⁸ difference frequency generation (DFG), and spontaneous parametric downconversion (SPDC).¹⁹ Because of sub-wavelength optical confinement, ultrahigh-efficiency frequency conversion, e.g., $2200\%–2600\% \text{ W}^{-1} \text{ cm}^{-2}$ normalized efficiencies for SHGs in the communication C-band, was reported with such nanophotonic waveguides that were several millimeters long.^{7,19} However, the measured efficiencies were only $\sim 60\%$ or lower than the

theoretically obtainable value. In this work, we provide a detailed description for the fabrication of high-quality periodically poled LNOI ridge waveguides, where the poling fidelity was actively monitored via confocal microscopy. The fabricated nanophotonic waveguide was characterized via SHG and DFG in the communication band, and the normalized conversion efficiencies were $\sim 80\%$ that of the theoretical values over the 6-mm waveguide length.

The fabrication process of the periodically poled LNOI waveguide could roughly be divided into two stages. The electric field poling technique was applied to obtain the ferroelectric domain structure; then, the sample was dry etched to form the ridge waveguide structure. The specific processing steps are shown in Fig. 1(a). First, a comb-shaped metal electrode was deposited on a 600-nm-thick X-cut LiNbO₃ thin film with Si as the substrate (NANOLN), and the spacing between the in-plane positive and negative electrodes was 6 μm . Then, high-voltage pulses were applied to fabricate the ferroelectric domain structure defined by the patterned electrode. After this, the electrode was removed and the ridge waveguide was fabricated using electron beam lithography (EBL) followed by an Inductively Coupled Plasma (ICP) etching process to produce the periodically poled LNOI ridge waveguide.

The conventional electric field poling technique²⁰ was applied to fabricate the domain structure in the LNOI. During and after the poling process, confocal second-harmonic (SH) microscopy was used to non-destructively characterize the inverted ferroelectric domain structure. The coercive field of the X-cut LNOI was higher than that of the bulk LiNbO₃ crystal. For bulk LiNbO₃, the coercive field was ~ 21 kV/mm, while for the LiNbO₃ thin film, it could be as high as 30 kV/mm.¹⁵ In

the domain structure fabrication process, the applied electric field was ~ 40 kV/mm and the pulse duration was several tens of milliseconds. The duty cycle of the fabricated structure was controlled by adjusting the number of applied high-voltage pulses. Figure 1(b) shows the evolution of the domain inversion with an increasing number of applied high-voltage pulses. When 2 pulses were applied, domain inversion began to occur; when the number of pulses reached 8, the domain gradually expanded outside the electrode area; when 12 pulses were applied, the duty cycle of the domain-inverted region was observed to be $\sim 50:50$ near the positive electrode; and excessive poling was observed when 40 pulses were applied, and the neighboring domains tended to merge. Through this intuitive and nearly real-time domain structure visualization scheme, we could control the number of pulses to obtain a periodically poled LiNbO₃ thin film with an optimized duty cycle. After the ferroelectric domain structure was fabricated, a ridge waveguide was obtained via dry etching of the LiNbO₃ thin film. The width of the inverted domain was 6 μm , while the width of the ridge was smaller. One advantage of this process sequence, i.e., poling followed by etching, was that we could select the poled region with the best poling quality for the subsequent ICP etching process, as shown in the dashed area in Fig. 1(d). The geometry of the ridge waveguide is shown in Fig. 1(e). The top width of the ridge waveguide was 1.4 μm and the etched depth was ~ 350 nm, with the angle of the waveguide sidewall being 60° . After periodic poling and dry etching, the chip was cleaved to expose the waveguide facets, and a subsequent focused ion beam (FIB) etching process was applied to polish both the waveguide facets.

The poling period was determined by the modal dispersion of the LiNbO₃ thin-film ridge waveguide, together with the momentum conservation condition. During the fabrication process, the errors for the etching depth and waveguide width were 20 nm and 100 nm, respectively, which led to a large deviation between the predicted and measured phase-matching wavelength because of the strong modal dispersion in such thin-film waveguides. To obtain a reliable poling period design, we prepared 11 periodically poled waveguides in parallel on the LNOI chip, and the poling periods of the waveguides were in the range 3.9–4.3 μm with equal intervals. In the experiment, we could switch among the channels to determine the most suitable one for phase-matching the given wavelength. In addition, the 11 waveguides were individually poled based on the active monitoring method to ensure good poling quality.

A schematic setup for the experiment is shown in Fig. 2. The pump wave from a continuous-wave (CW) Ti:sapphire laser was gathered into a single-mode fiber and then combined with the signal from a CW fiber laser (SANTECH, TSL-550) using a wavelength division multiplexer (WDM). The polarization of the interacting three modes was chosen to be TE, which corresponds to a type-0 phase-matching diagram, and the pump and the signal pass through the polarization controller to ensure excitation of the TE modes in the waveguide. Then, both beams were coupled to the thin film waveguide using a lensed fiber and the fiber-to-chip coupling loss was ~ 10 dB. The light was coupled out of the waveguide using an aspherical mirror with an optimized focal length of 4 mm, and the coupling loss off the chip was estimated to be ~ 1 dB (including Fresnel reflection at the end facet). Filters were placed behind the aspherical mirror for the measurement of the generated waves.

The SHG performance was characterized using a waveguide with a poling period of 4.3 μm on the nanophotonic chip. The CW fiber

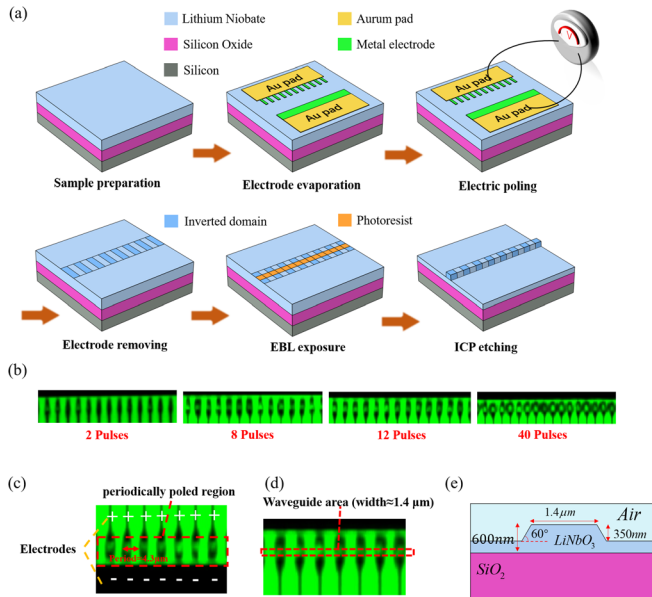


FIG. 1. (a) Fabrication procedure for the periodically poled LNOI ridge waveguide. (b) Evolution of inverted domain growth with the number of applied high-voltage pulses. (c) Magnified view of the domain-inverted region in the LiNbO₃ thin film recorded via SH confocal microscopy, where domain inversion occurred in the red dotted box. (d) Ridge waveguide was selectively fabricated in the domain-inverted region with a duty cycle close to 50:50, as shown in the red dotted box. (e) The cross section of the LNOI ridge waveguide.

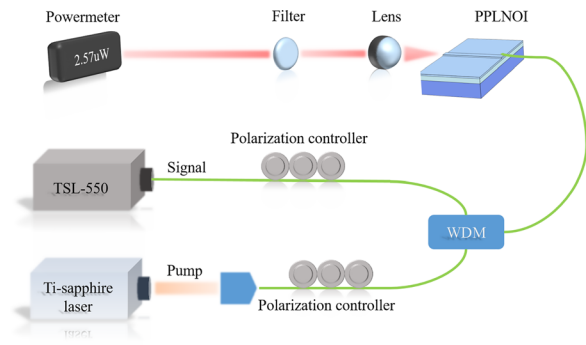


FIG. 2. Schematic experimental setup.

laser, which is tunable near 1470 nm, was utilized as the fundamental light source in the measurement. The measured and theoretical wavelength tuning curves are shown in Fig. 3(a). The first zeros of the ideal curve were at 1467 nm and 1473 nm, while the measured curve had two non-zero dips around the two points, which can be attributed to the excitation of the high-order modes in the SHG. The full width at half maximum (FWHM) of the spectrum was ~ 4 nm, which is slightly larger than the predicted value of 3.2 nm. When the wavelength of the fundamental wave (FW) was tuned to 1469.6 nm, a maximum output power of $1.62 \mu\text{W}$ for the SH wave was obtained, with an FW power of $397 \mu\text{W}$. Because of fabrication errors, the observed SHG wavelength differed significantly from the calculated value of 1520 nm. Figure 3(b) shows the output power of the SH as a function of the square of the power of the FW, which is a linear relation in theory. The normalized SHG conversion efficiency can be calculated according to $\eta_{SHG} = P_{SH}/(P_{FW}^2 \cdot L^2)$, in which P_{FW} and P_{SH} represent the powers of the FW and SH waves, respectively, and $L = 6\text{mm}$ is the length of the poled waveguide. Using the fitted slope from Fig. 3(b), the normalized SHG conversion efficiency was calculated to be $3061\% \text{ W}^{-1} \text{ cm}^{-2}$, which is 83% of the theoretical efficiency $3700\% \text{ W}^{-1} \text{ cm}^{-2}$. The lower maximum efficiency was mainly caused by the film thickness gradient over the 6 mm waveguide length.⁷ The results of the SHG measurement revealed the high poling quality of the fabricated periodically poled LNOI ridge waveguide. Furthermore, we tested the SHG performance of the 11 waveguides on the chip, and the normalized efficiencies of all these waveguides were in the range of 60%–80%

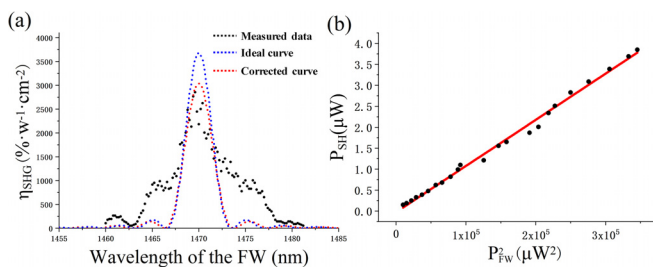


FIG. 3. (a) Measured wavelength tuning curve for the SHG in the periodically poled LNOI ridge waveguide (black dotted curve) and the theoretical curves. The blue and red dotted curves correspond to the ideal and corrected transfer functions, respectively. (b) Quadratic power dependence of the SH wave on the FW.

of the theoretical value, indicating the reliability and repeatability of the fabrication process.

DFG was carried out using the same waveguide as that for the SHG. We fixed the wavelength of the signal at 1400 nm and tuned the wavelength of the pump wave from 730 to 740 nm, and the normalized DFG conversion efficiency varied with the wavelength of the pump, as shown in Fig. 4(a). The wavelength of the output idler was tuned from 1520 to 1570 nm, covering the entire spectral range of the C-band. When the wavelength of the pump was tuned to be 735.5 nm, the power of the generated idler at 1549.6 nm was $2.57 \mu\text{W}$, while the power of the pump wave and signal wave was 212 and $326 \mu\text{W}$, respectively. According to the definition of the normalized DFG efficiency $\eta_{DFG} = P_i/(P_p \cdot P_s \cdot L^2)$,²¹ where $P_{p,s,i}$ are the powers of the pump, the signal, and the generated idler, respectively, the normalized conversion efficiency at the maximum output was $10300\% \text{ W}^{-1} \text{ cm}^{-2}$, which is $\sim 75\%$ that of the theoretical value $14000\% \text{ W}^{-1} \text{ cm}^{-2}$. The power relationship of the DFG process was characterized as well; when the wavelength of the pump and signal light was fixed at 735 nm and 1397.5 nm, respectively, the corresponding wavelength of the idler was 1550 nm. Figure 4(b) gives the relation of the power dependence of the idler on the product of the pump and the signal, which indicates a nearly linear relationship. In addition, we measured the DFG tuning characteristics when the wavelength of the pump was fixed at 737 nm, while the signal wavelength was scanned from

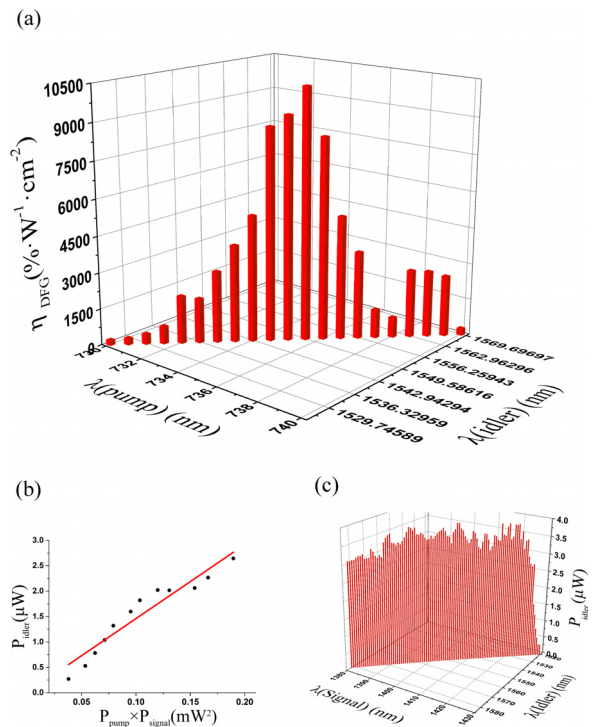


FIG. 4. Results of the DFG measurements. (a) The recorded normalized DFG efficiency as the wavelength of the pump is tuned from 730 to 740 nm with a fixed signal at 1400 nm. (b) Linear scaling of the power of the idler on the product of the power of the pump and signal. (c) Output power of the idler at a fixed pumping wavelength (737 nm), while the signal is tuned from 1380 to 1430 nm.

1380 to 1430 nm in the E-band. In this case, the wavelength of the idler was tuned in the C-band from 1524 to 1581 nm, as shown in Fig. 4(c).

To conclude, we fabricated a periodically poled LNOI using the electrical field poling technique followed by dry etching to form a ridge waveguide. The duty cycle was controlled to be close to 50:50 by adjusting the number of applied high-voltage pulses. SH confocal microscopy was used to actively reveal the inverted ferroelectric domain structure. The periodically poled LNOI waveguide was characterized by SHG at 1470 nm with the normalized conversion efficiency being $3061\% \text{ W}^{-1} \text{ cm}^{-2}$, which is $> 80\%$ of the theoretical value. In addition, DFG was realized with a pumping wavelength at ~ 730 nm in the visible part of the spectrum, and the spectral tuning range of the generated idler in the C-band was ~ 50 nm. The normalized DFG conversion efficiency reached about 75% of the predicted one. The results obtained in this work show that active monitoring of the poling fidelity during the fabrication process can yield LiNbO_3 nanophotonic devices with conversion efficiencies comparable to the theoretically obtainable values, which can promote the use of LNOI for integrated photonic applications. Because of the strong geometric dispersion and the fabrication errors, the LNOI platform needs further development to improve the reliability and repeatability, thus alleviating a substantial testing in the creation of devices. The fabrication process should be improved, and one possible solution is to use a different process sequence, e.g., periodical poling after ridge waveguide fabrication; thus, a more accurate poling period can be obtained based on the measured geometric parameters of the nanophotonic waveguide from the previous procedure. Moreover, designing of new photonic structures with high tolerance to the fabrication errors might be an alternative direction.

This work was supported by the National Key R&D Program of China (Nos. 2019YFA0705000 and 2017YFA0303700), the National Natural Science Foundation of China (NSFC) (Nos. 11674171, 91950206, 11627810, and 51890861), the Leading-edge Technology Program of Jiangsu Natural Science Foundation

(No. BK20192001), and the Key R&D Program of Guangdong Province (No. 2018B030329001).

REFERENCES

- ¹E. H. Turner, *Appl. Phys. Lett.* **8**, 303 (1966).
- ²K.-K. Wong, *Properties of Lithium Niobate* (IET, 2002), p. 28.
- ³H. Jin, F. M. Liu, P. Xu, J. L. Xia, M. L. Zhong, Y. Yuan, J. W. Zhou, Y. X. Gong, W. Wang, and S. N. Zhu, *Phys. Rev. Lett.* **113**, 103601 (2014).
- ⁴M. Bazzan and C. Sada, *Appl. Phys. Rev.* **2**, 040603 (2015).
- ⁵M. B. He, M. Y. Xu, Y. X. Ren, J. Jian, Z. L. Ruan, Y. S. Xu, S. Q. Gao, S. H. Sun, X. Q. Wen, L. D. Zhou, L. Liu, C. J. Guo, H. Chen, S. Y. Yu, L. Liu, and X. L. Cai, *Nat. Photonics* **13**, 359 (2019).
- ⁶C. Wang, M. Zhang, X. Chen, M. Bertrand, A. Shams-Ansari, S. Chandrasekhar, P. Winzer, and M. Lončar, *Nature* **562**, 101 (2018).
- ⁷C. Wang, C. Langrock, A. Marandi, M. Jankowski, M. Zhang, B. Desiatov, M. M. Fejer, and M. Lončar, *Optica* **5**, 1438 (2018).
- ⁸A. Rao, K. Abdelsalam, T. Sjaardema, A. Honardoost, G. F. Camacho-Gonzalez, and S. Fathpour, *Opt. Express* **27**, 25920 (2019).
- ⁹Y. L. Zheng, Z. W. Fang, S. J. Liu, Y. Cheng, and X. F. Chen, *Phys. Rev. Lett.* **122**, 253902 (2019).
- ¹⁰C. H. Lu, B. Zhu, C. Y. Zhu, L. C. Ge, Y. Liu, Y. P. Chen, and X. F. Chen, *Chin. Opt. Lett.* **17**, 072301 (2019).
- ¹¹C. Wang, X. Xiong, N. Andrade, V. Venkataraman, X. F. Ren, G. C. Guo, and M. Lončar, *Opt. Express* **25**, 6963 (2017).
- ¹²L. Cai, Y. Wang, and H. Hu, *Opt. Commun.* **387**, 405 (2017).
- ¹³C. Zhu, Y. Chen, G. Li, L. Ge, B. Zhu, M. Hu, and X. Chen, *Chin. Opt. Lett.* **15**, 091901 (2017).
- ¹⁴C. Wang, Z. Y. Li, M. H. Kim, X. Xiong, X. F. Ren, G. C. Guo, N. F. Yu, and M. Lončar, *Nat. Commun.* **8**, 2098 (2017).
- ¹⁵L. Chang, Y. F. Li, N. Volet, L. R. Wang, J. Peters, and J. E. Bowers, *Optica* **3**, 531 (2016).
- ¹⁶J. Y. Chen, Z. H. Ma, Y. M. Sua, Z. Li, C. Tang, and Y. P. Huang, *Optica* **6**, 1244 (2019).
- ¹⁷J. J. Lu, J. B. Surya, X. W. Liu, A. W. Bruch, Z. Gong, Y. T. Xu, and H. X. Tang, *Optica* **6**, 1455 (2019).
- ¹⁸G. Z. Li, Y. P. Chen, H. W. Jiang, and X. F. Chen, *Opt. Lett.* **42**, 939 (2017).
- ¹⁹J. Y. Chen, Y. M. Sua, Z. H. Ma, C. Tang, Z. Li, and Y. P. Huang, *OSA Continuum* **2**, 2914 (2019).
- ²⁰S. N. Zhu, Y. Y. Zhu, Z. Y. Zhang, H. Shu, H. F. Wang, J. F. Hong, C. Z. Ge, and N. B. Ming, *J. Appl. Phys.* **77**, 5481 (1995).
- ²¹M. H. Chou, J. Hauden, M. A. Arbore, and M. M. Fejer, *Opt. Lett.* **23**, 1004 (1998).